Water Resources Research

RESEARCH ARTICLE
10.1029/2023WR035475

Spatiotemporal Variability of Hyporheic Flow in a Losing River Section

N. Simon[1,2], O. Bour[1], J. Heyman[1], N. Lavenant[1], C. Petton[1], and A. Crave[1]

[1]CNRS, Univ Rennes, Geosciences Rennes – UMR 6118, Rennes, France, [2]Department Urban and Environmental Engineering, Hydrogeology and Environmental Geology, Liège Université, Sort Tilman, Belgium

Key Points:

- Active-Distributed Temperature Sensing was used in a lowland stream to assess and map the spatiotemporal variability of stream infiltration
- An innovative field setup and a new methodology was developed to remove ambient temperature variations from the raw temperature signal
- Results suggest relatively homogeneous streambed properties and show remarkable stability of hyporheic flow during few years

Supporting Information:

Supporting Information may be found in the online version of this article.

Correspondence to:

N. Simon,
nataline.simon2@gmail.com

Citation:

Simon, N., Bour, O., Heyman, J., Lavenant, N., Petton, C., & Crave, A. (2024). Spatiotemporal variability of hyporheic flow in a losing river section. *Water Resources Research*, *60*, e2023WR035475. https://doi.org/10.1029/2023WR035475

Received 1 JUN 2023
Accepted 22 APR 2024

Author Contributions:

Conceptualization: N. Simon, O. Bour, J. Heyman, N. Lavenant, A. Crave
Formal analysis: N. Simon
Funding acquisition: O. Bour, A. Crave
Investigation: N. Simon, O. Bour, J. Heyman, N. Lavenant, C. Petton, A. Crave
Methodology: N. Simon
Project administration: O. Bour, A. Crave
Resources: N. Lavenant, C. Petton
Software: N. Simon
Supervision: O. Bour
Validation: N. Simon, O. Bour
Visualization: N. Simon
Writing – original draft: N. Simon

Abstract Characterizing the spatiotemporal variability of water fluxes at the stream-groundwater interface is extremely challenging due to the lack of methods for estimating hyporheic flows at different scales. To address this, we demonstrate the potential of Active-Distributed Temperature Sensing (DTS) methods for measuring and mapping hyporheic flow in a lowland stream. Experiments were conducted by burying a few hundred meters of heatable Fiber-Optic cables within streambed sediments in a large meander, where permanent stream-losing conditions are observed along the stream reach. We propose a new methodology to filter ambient temperature variations along the heated section of the DTS cable and to extend the application of Active-DTS to losing streams. After data processing, the results show that, along lateral and longitudinal stream profiles, both thermal conductivity and water flux values follow normal distributions with relatively small standard deviations. Hyporheic fluxes vary by one order of magnitude. The absence of correlation between water fluxes within the hyporheic zone and streambed topography variations suggests that the variability is mainly controlled by local streambed heterogeneities. This means that the spatiotemporal variability of fluxes may be used as a marker of the variability of streambed hydraulic conductivities. The relatively low spatial variability (one order of magnitude) in hyporheic flow suggests a small variability of streambed properties. This is an important result for calibrating models assessing hyporheic processes, in which the hydraulic conductivity distribution is generally assumed. Additionally, measurements made over three years yield similar estimates showing the remarkable stability of hyporheic flows through time.

Plain Language Summary Characterizing the interactions between groundwater and surface water is extremely challenging although such interactions control water quality and ecosystems resilience to climate changes. Here, we used an innovative approach based on heated fiber optic cables, called Active-Distributed Temperature Sensing, to image the spatial variability of hyporheic fluxes in a lowland stream. Our results show that the instrumental developments as well as the data processing methodology are very robust to accurately measure in-situ the thermal conductivity of stream sediments and hyporheic fluxes within the streambed. Interestingly, groundwater flux variability was found relatively limited and not correlated to the morphology of the riverbed. In addition, measurements made over three years yield similar estimates showing the excellent reproducibility of the measurements and the remarkable stability of hyporheic flows through time. These results shed new light about the spatial and temporal variability of hyporheic fluxes in a lowland river.

1. Introduction

The stream-groundwater exchanges play a key role in the water cycle and in the preservation of riparian habitats and groundwater-dependent ecosystems (Frei et al., 2019; Jones & Mulholland, 2000; Kalbus et al., 2006). Characterizing these exchanges is a key concern for the efficient management of water resources. However, in practice, assessing stream-groundwater exchanges is difficult, especially in lowland rivers. In such cases, the hydraulic gradient between the stream and the aquifer controls exchanges at large-scales while multiple and multi-scale morphological features and geological heterogeneities induce complex flow patterns at the surface water-streambed interface (Flipo et al., 2014; Krause et al., 2022; Sophocleous, 2002; Stonedahl et al., 2010; Woessner, 2000; Wörman et al., 2002). River morphologies ranging from small bedforms to large meanders (Wondzell et al., 2019) can control flow paths through the riverbed (Boano et al., 2006; Gomez-Velez & Harvey, 2014; Revelli et al., 2008). Thus, spatial variations in bed forms (Boano et al., 2007; Cardenas & Wilson, 2007; Harvey & Bencala, 1993; Storey et al., 2003), in channel bends (Boano et al., 2006, 2010; Cardenas, 2008b, 2009; Gomez-Velez & Harvey, 2014) and/or in large-scale surface topography (Sophocleous, 2002; Tóth, 1963; Wörman et al., 2007) induce complex flow paths patterns occurring at multiple scales

Writing – review & editing: N. Simon, O. Bour, J. Heyman, A. Crave

within streambeds and river banks but also through meanders and floodplains. Furthermore, the spatial heterogeneity of hydraulic and hydrogeological properties of sediments may also highly affect flow paths at the stream-groundwater interface (Genereux et al., 2008; Krause et al., 2022; Laube et al., 2018).

This results in general in complex flow patterns occurring in the hyporheic zone, where stream water and groundwater of variable composition and age mix (Bencala, 1993; Boano et al., 2014; Hester et al., 2017; Krause et al., 2009, 2011). Due to river water level fluctuations, hyporheic flows are also expected to vary in time over orders of magnitude, from hours to years (Cardenas, 2008a; Flipo et al., 2012; Hester et al., 2019; Kaufman et al., 2017; Singh et al., 2019, 2020; Trauth & Fleckenstein, 2017; Wu et al., 2018). These spatiotemporal fluctuations significantly complicate the observation of hyporheic processes in the field. Thus, distinguishing hyporheic from groundwater flows can be challenging, especially because regional groundwater flow patterns also influence patterns and rates of hyporheic exchange (Cardenas, 2008a; Wörman et al., 2007).

Modeling (Boano et al., 2010; Cardenas et al., 2004; Gomez-Velez & Harvey, 2014; Shanafield et al., 2010) and laboratory experiments (Arnon et al., 2010; Fox et al., 2014, 2016; Salehin et al., 2004) have provided a better understanding of the mechanisms controlling hyporheic fluxes. However, the models often fail to reproduce field observations adequately. For example, several mechanistic models have investigated the effects of geologic heterogeneity on hyporheic flow and of riverbed heterogeneity on stream-groundwater interactions (Brunner et al., 2017; Fleckenstein et al., 2010; Hermans et al., 2023; Singh et al., 2020; Trauth & Fleckenstein, 2017). When applied in the field, these mechanistic model poorly described field observations (Bardini et al., 2013; Cardenas et al., 2004; Laube et al., 2018). Attempting to explain such divergence, Krause et al. (2022) suggested that boundary conditions of models do not appropriately represent the mechanisms governing hyporheic flow dynamics in a real-world context. To implement realistic boundary conditions of physical models, it is crucial to use field methods with the ability to image the effect of heterogeneities at high resolution within the hyporheic zone over a range of spatial and temporal scales.

Field studies often rely on the characterization of streambed hydraulic conductivities, whose in-situ measurements are typically taken at the point-scale, leading to significant estimate uncertainty (Landon et al., 2001). Heat has also been used as a tracer to assess hyporheic flow with the development of vertical temperature profiles (Constantz, 2008) and heat pulse probes (Banks et al., 2018; Lewandowski et al., 2011; Zlotnik & Tartakovsky, 2018). However, while these approaches are efficient to assess hyporheic fluxes locally, they do not constrain spatial variability of the fluxes, unless surveys are repeated (Schmidt et al., 2006). This is time-consuming and may still yield spatial biases based on the constraints of such sensors. To overcome these problems, Distributed Temperature Sensing (DTS) technology can be used to collect high resolution temperature measurements along Fiber Optic (FO) cables. By installing FO cables at different depths, these data can then be used to estimate the spatial variability of vertical water fluxes (Mamer & Lowry, 2013; Shanafield et al., 2018). However, the installation of FO cables at different depths in the hyporheic zone is technically challenging.

In this context, the Active-Distributed Temperature Sensing (Active-DTS) technique is attractive as it can provide high-resolution measurements of saturated subsurface flows. Active-DTS methods rely on heating of a FO cable while monitoring the resulting temperature rise at high spatial (from 10 cm to meters) and temporal resolution (every 30 s). In saturated sediments, the temperature increase is primarily dependent on the thermal conductivity of the porous media and on the water flux (estimated by the Darcy flux) through the porous media (Bense et al., 2016; del Val et al., 2021; des Tombe et al., 2019; Simon et al., 2021; Zhang et al., 2023). Water flow leads to advective heat transfer that dissipates the injected heat away from the cable more quickly than conduction alone, reducing the observed increase in temperature.

The use of Active-DTS measurements for the assessment of groundwater-surface water interactions in the hyporheic zone is relatively new. The first use of Active-DTS in such context was proposed by Kurth et al. (2015), who showed the possibility of detecting lower and higher flow rates along the heated cable. These vertical flux estimates are limited to a point-scale of discharge/infiltration. Briggs et al. (2016) then proposed to quantify vertical fluxes in streambed sediments using active heating of wrapped fiber-optic sensors, but this also provides only local discharge/infiltration assessment. More recently, Simon et al. (2022) buried a heatable FO cable into the streambed sediments of a headwater stream to assess the groundwater discharge. Results showed a large variability of both thermal conductivities and upward fluxes along a relatively short longitudinal profile. Banks et al. (2022) used horizontal directional drilling for installing heated FO cables buried 5 m below a losing reach of

a braided river. They found a relatively small spatial variability of river losses to the underlying aquifer system (Banks et al., 2022).

Here, we present results of a novel Active-DTS study in the hyporheic zone of a predominantly losing river section. The aim is to estimate and map the spatiotemporal variability of water fluxes and of streambed sediment properties at high resolution (with a measurement point every 12.7 cm) in a large lowland river. To do this, we designed an innovative field setup, consisting of two fiber-optic cables buried along several hundred meters within the river sediments. In addition, we present a new approach to remove ambient temperature variations from the measured temperature signal to generalize the application of Active-DTS measurements to losing streams.

2. Experiment

2.1. Experimental Site

Active-DTS measurements were conducted at the Signy experimental site located in the lowland reach of the Sélune River in Normandy, France (Figures 1a and 1b). The Sélune River drains a 1,083 km^2 catchment before flowing into Mont-Saint-Michel Bay in north-western France (Fovet et al., 2020). The experimental site is located ∼15 km from the final outlet to the sea and ∼ four km downstream of a major dam (Figure 1a). The drainage area upstream from the study site is ∼777 km^2. In this upstream area of the catchment, the Sélune River is a high-order and large stream (15–20 m width) characterized by a floodplain and meanders, with lower streambed gradients compared to the upper reaches. The experimental site consists of a 34-ha meander with east to west flow (Figure 1b). The annual average discharge at the Signy experimental site is 9.5 $m^3.s^{-1}$, based on data acquired from a local hydrometric station. Photos of the experimental site are provided in Supporting Information S1 (Figure S1).

The alluvial aquifer located across the neck of the meander lobe has been used for municipal water supply since the 1970s, with three pumping wells providing 1,500 m^3 of water in total per day (Figure 1b). Data from a piezometer network consisting of 10 piezometers across the meander, show that groundwater head is always lower than stream level, indicating permanent stream-losing conditions. The pumping induces significant hydraulic gradients between the stream and the aquifer (around 8–9 $\times 10^{-3}$ $m.m^{-1}$), which considerably simplifies the flow complexity in the hyporheic zone. This assumption is consistent with groundwater level monitoring across the neck, which displays rapid groundwater response to stream stage variations, indicating the hydraulic connection between the stream and the alluvial aquifer. Thus, the response time between any stream water level variation and the related groundwater level variation measured in P1, which is the closest piezometer of the bank where the experiment was conducted (Figure 1b), is around 10 min.

2.2. Active-DTS Experiments

2.2.1. Experimental Setup

Active-DTS experiments were performed in the southern part of the meander (Figure 1b), where three piezometers were installed to monitor groundwater level changes. This section of the meander was selected because of stream/riverbank accessibility. Electricity is also available at the hydrometric station. Figure 1c shows the experimental setup consisting of two FO cables buried within the streambed sediments at 10 cm depth. Experiments were conducted using a 3.8-mm-diameter cable (BruSens cable; reference LLK-BSTE 85°C) containing four multimode 50/125-µm fibers, protected by steel armoring and a plastic jacket. For a long-term deployment, this type of cable presents the advantage of being particularly resistant to damage induced by flood events or animals. Moreover, electricity can be injected within the steel armoring of the cable, which allows heating the FO cable. In this configuration, each FO cable can be heated along some sections of the cable, while non-heated sections can be used to monitor riverbed temperature. Moreover, the distance between the heated armoring and the fibers does not vary along the cable.

FO1 consisted of a 167 m-long buried cable with three electrical connections, F1-3, F1-2 and F1-1, which allowed for varying heat injection points along the cable. A toggle switch allowed for three sections of the cable to be heated. These sections of cable are referenced as F1-3/F1-2 (65 m length), F1-2/F1-1 (55 m length), and F1-3/F1-1 (120 m length) based on the section of the cable between electrical connections (Figure 1c). Whatever the section heated, streambed temperature variations were continuously monitored in the sections that were not heated and along the 47 m of buried cable located outside the heated sections.

10.1029/2023WR035475

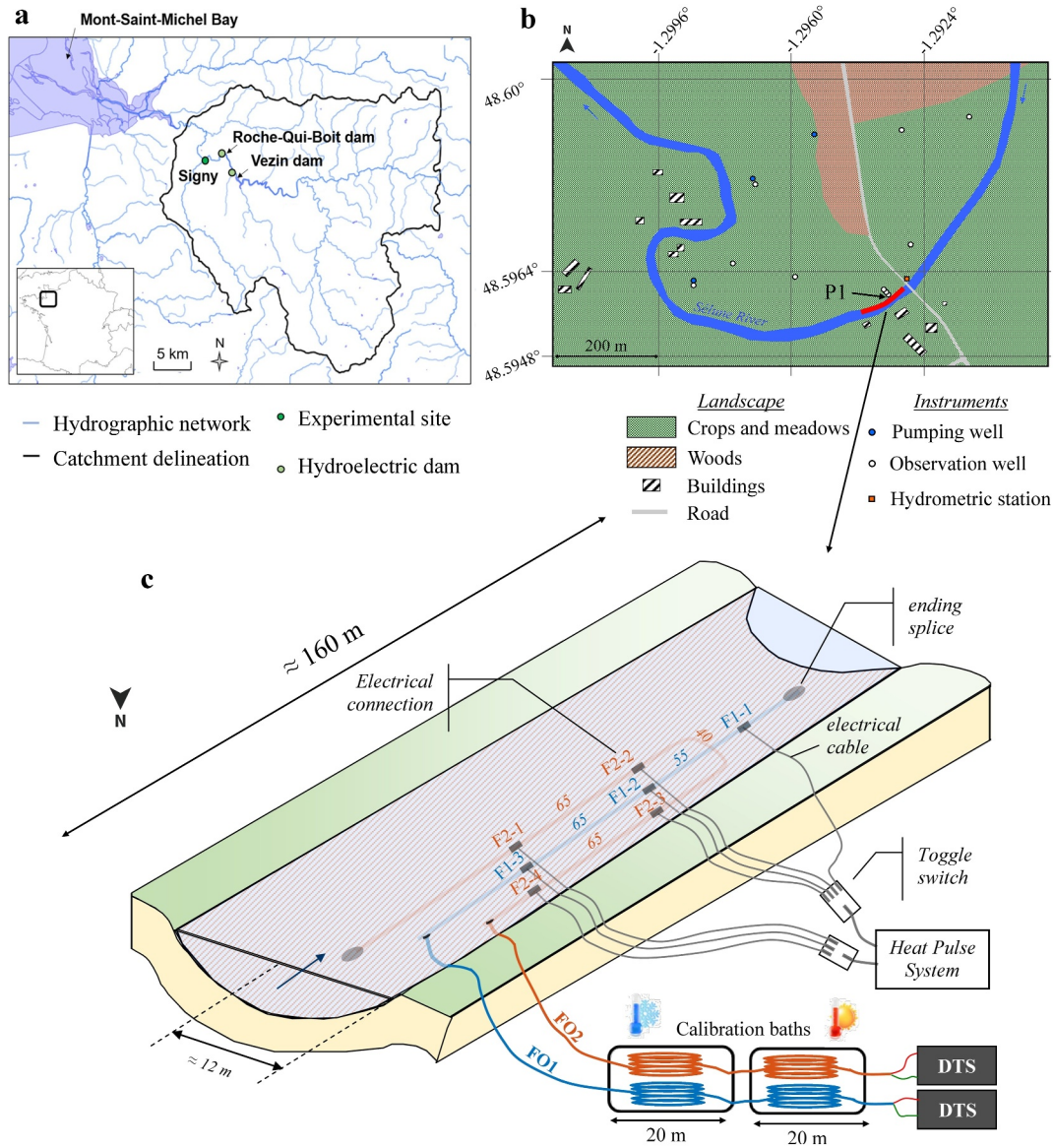

Figure 1. (a) Map of the Sélune catchment indicating the location of the experimental site of Signy [modified from Fovet et al. (2020)]. The inset map shows the location of the Sélune catchment in France. (b) Map of the experimental site of Signy. Active-DTS measurements were made in the southern part of the meander (red line). Seven observation wells and three pumping wells are found within the meander. In addition, three piezometers were installed near the riverbank (P1 being the closer of the bank). (c) Experimental setup of the Active-DTS experiments conducted in Signy. Two FO cables (called FO1 and FO2) were buried within the streambed sediments at 10 cm-depth and heated sections of the cables were connected separately to a heat pulse unit and controlled using a toggle switch. The total length of buried FO cables is about 374m.

The second buried FO cable, FO2, was installed in a U-shape to get three parallel heatable cable sections at different distances from the riverbank. The distance between these sections varied between 2 and 4 m. This innovative experimental setup allowed us to study both the longitudinal variability of surface water infiltration over the whole heatable section (120 m) and the lateral variability at different distances from the riverbank (Figure 1c). FO2 is a 207 m-long buried cable with four electrical connections, F2-4, F2-3, F2-2 and F2-1. The toggle switch allowed for five sections of the cable to be heated. These sections of cable are referenced as F2-4/F2-3 (65 m length), F2-3/F2-2 (40 m length), F2-2/F2-1 (65 m length), F2-4/F2-2 (105 m length) and F2-3/F2-1 (105 m length) based on the section of the cable between electrical connections (Figure 1c).

A plow developed for the installation of FO in soils and sediments, was used to bury the FO cables within the streambed at 10 cm depth (Figure S1 in Supporting Information S1). The installation of the whole setup required one week with a team of five people. During the installation, GPS measurements were made to precisely locate the cables. The burial depth of the cables was also controlled each half meter by controlling the depth of the plow in the streambed. During the deployment, the height of the water column was also measured using a ruler all along the cable, which allowed mapping the riverbed morphology and the alternance of riffles and pools. Riffle-pool sequences were along ~50 m of the FO1 cable (see Figure S4b in Supporting Information S1).

2.2.2. DTS Measurements

Two DTS units were used for recording temperature variations (Figure 1c): one Silixa Ultima S instrument configured to collect data at a sampling resolution of 12.7 cm, with a 20 s time interval and one Silixa XT-DTS instrument configured to collect data at a sampling resolution of 25.4 cm and a 20 s time interval. Both units were configured in a double-end configuration (van de Giesen et al., 2012) and calibrated using one cold calibration bath, a box filled with wetted ice, and one warm calibration bath, equipped with a heating resistor. About 20 m of FO cable were submerged in each calibration bath. Following Simon et al. (2020), effective spatial resolutions of DTS measurements along the cable are estimated to vary between 51 and 67 cm for the Silixa Ultima S instrument and between 66 and 90 cm for the Silixa XT-DTS instrument. To heat a specific section of the buried FO cables, a Heat Pulse System was used to inject electricity in the electric cables/FO cable system. Thus, the setup of the experiment allowed heating only one section of cable at time, with heating periods varied between 4 and 52 hr. As the spatial resolution of the Silixa Ultima S unit is higher, this instrument was systematically used to monitor temperature variations along the actively heated section of the FO. Concurrently, the Silixa XT-DTS unit was used to monitor temperature variations along the second non-heated FO cable.

To study temporal variability of hyporheic flow, surveys were repeated under different meteorological and hydrological conditions. FO cables were buried before the first experimental week and have remained in place for 2 years, the entire duration of the experiment. We assume that the eight weeks time period between the cable installation and the first experiment was sufficient for the riverbed recovery as the sediment resettled around the cable. Heated sections of the FO cable were tested over four weeks, in November 2017, in April 2018, in September 2018 and in September 2019, during which all heated sections were tested. Losing conditions were systematically observed over these time periods. The first and second experimental weeks (Nov-17, April-18) experienced similar hydrological conditions and were relatively wet periods. At that time, the piezometric level in P1 and the stream water level both experienced significant fluctuations, mainly due to upstream dam releases. The groundwater level follows the stream level fluctuations. This is due to the hydraulic connection between the stream and the alluvial aquifer. Thus, despite rapid and significant changes in the river level, the hydraulic head difference between the stream and P1 (Δh) does not vary significantly over time. In contrast, the third and fourth experimental weeks (Sept-18, Sept-19) were relatively dry periods. At that time, the piezometric level in P1 was around 10.23 m and the difference between the stream and P1 (Δh) was around 7.5 cm. Details about the hydrological conditions occurring during the four weeks of experiment conducted and about heating periods (durations and injected power [$W.m^{-1}$] are provided in Supporting Information S1 (Figure S2).

3. Data Processing

3.1. Data Acquisition and Pre-Processing

Examples of raw temperature profiles recorded along cable FO1 are provided in Supporting Information S1 (Figure S3). Data processing involved two primary steps before interpretation consisting of removing non-buried sections and verifying the consistency of measurements. The first step removed non-buried sections from temperature profiles using GPS measurements made during the burial of the cable. The non-buried sections were easily identified as the temperature increase observed during heating periods features rapid temperature stabilization, as observed by Read et al. (2014) and Simon et al. (2022). In a second step, to verify the consistency of temperature measurements, we applied the following process. The capacity of measuring small-scale temperature gradients depends on the DTS unit and the spatial resolution of measurements (Simon et al., 2020). If temperature changes occur at a scale smaller than the spatial resolution of measurements, the measured temperature may be lower or higher than the true temperature. This can then lead to an estimated water flux being overestimated or underestimated. Therefore, such measurements are not considered although they could be interpreted. To identify

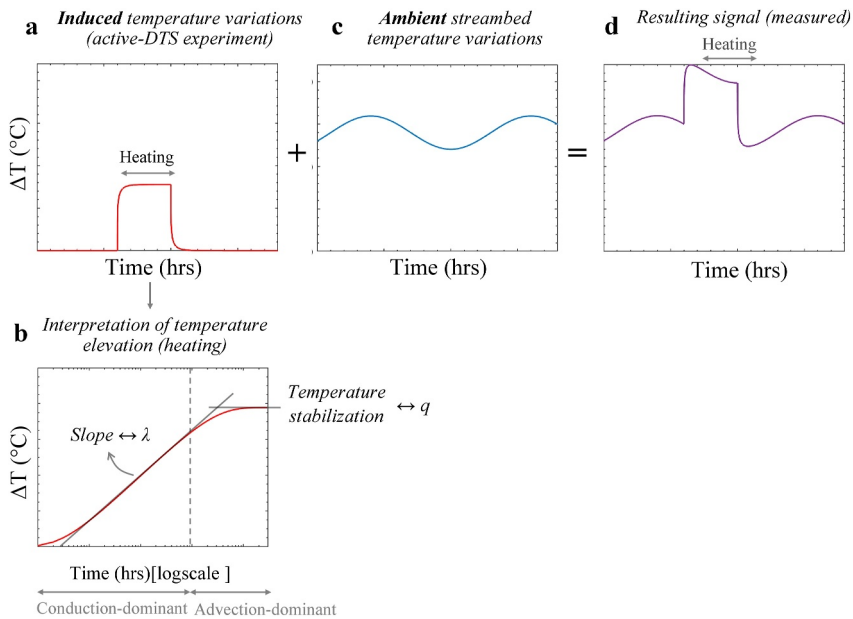

Figure 2. (a) Theoretical curve of temperature variations induced during Active-DTS experiments. (b) Data interpretation of the temperature increase in semi-log scale to estimate both thermal conductivity of sediments (λ) and water flux (q). (c) Example of ambient temperature variations which could be observed in streambed sediments under losing conditions. (d) Resulting temperature variations that could be recorded while conducting Active-DTS experiments in losing conditions.

such measurements, we applied the derivative method, which consists of calculating the derivative of the temperature with respect to distance to highlight abrupt temperature changes that cannot be efficiently measured by the DTS unit (Simon et al., 2020).

3.2. Theoretical Background for Data Interpretation

Previous studies validated the use of heated FO cables for estimating water fluxes in porous media (del Val et al., 2021; des Tombe et al., 2019; Simon et al., 2021). The principle of the method consists of injecting an artificial heat source in a saturated porous media and continuously monitoring the associated temperature increase (ΔT) over time (Figure 2a). Conduction and advection are the two main heat transfer processes that control the temperature evolution during heat injection. Initially, the temperature rise is mainly controlled by conduction, which depends on the thermal conductivity of the material that controls the diffusion of thermal energy within the solid matrix. In a semilogarithmic plot (Figure 2b), the "induced" temperature evolution follows a gradual and continuous increase of temperature during this conduction-dominant period. Subsequently, the emitted heat is mainly dissipated by advection (Diao et al., 2004; Simon et al., 2021). The dissipation of the heat produced by flowing water through the porous media results in the temperature stabilization for late time (Figure 2b). Therefore, the magnitude of the temperature increase at steady-state conditions depends on water flow: the higher the water flux, the higher the heat dissipation by advection and thus the lower the temperature increase.

The interpretation of the induced temperature evolution consists of a two-steps reflecting the two heat transfer mechanisms controlling the thermal response. Here, we briefly recall the main steps to infer the flux from the temperature signal. The first step is to estimate the thermal conductivity of the porous media by analyzing the temperature increase measured during the conduction-dominant period. During this period, the slope of the linear regression between ΔT and ln(t) (Figure 2b) mainly depends on the thermal conductivity of the porous media, meaning that its value is independent of the flow velocity. Thus, the temperature increase measured during the conduction-dominant period can be simulated using the 1-D MILS (Moving Instantaneous Line Source) analytical model, initially introduced by Carslaw and Jaeger (1959), by considering $q = 0$ m.s^{-1}. Once thermal conductivity (λ) is estimated, the MILS model can be used to reproduce the subsequent temperature evolution. Groundwater flux can be determined based on the late-time temperature behavior and temperature stabilization, derived from the independent variable of thermal conductivity. Long heating periods (>4 hr) were used to ensure

stable temperatures and accurate flux estimates. Finally, as Simon, Bour, Lavenant, et al. (2023) showed that water fluxes variations over time may be monitored through Active-DTS measurements, we used longer heating periods (up to 52 hr) to monitor the possible effect of dam release, which induced rapid changes in stream level, on hyporheic flow. Further details about the method used for data interpretation can be found in Simon et al. (2021) and Simon and Bour (2023).

The ADTS toolbox can be used to automatically interpret temperature increases recorded in all heated sections from Active-DTS measurements (Simon & Bour, 2023). This toolbox estimates both the thermal conductivity of the surrounding material and the water flux and their uncertainties for each measurement point. Note also that the data interpretation considers that the electricity injection through the steel armoring of the FO cable induces a significant temperature increase in the first minutes of the experiment (del Val et al., 2021; Simon et al., 2021). This temperature elevation due to heat conduction through the FO cable was calibrated with lab experiments (Simon et al., 2021) and adjusted for each heating period depending on the electrical power injected. Thus, the temperature increase due to the cable heating was estimated 3.32°C at 7 $W.m^{-1}$ and 11.8°C at 24.96 $W.m^{-1}$, which is in good agreement with the results of Simon and Bour (2023) using similar FO cables.

3.3. Application of Active-DTS in Losing Streams

Water flux estimates from Active-DTS experiments rely on the interpretation of induced temperature variations (Figures 2a and 2b) that are temperature increases resulting from the artificial injection of heat into the porous media. This means that ambient temperature variations must be negligible to correctly interpret the results of the heating experiment. In gaining streams, sediment temperature shows negligible diurnal variations indicating the temperature of the water discharging into a stream is generally relatively constant (Constantz, 2008). In such cases, temperature variations recorded during heating experiments may be exclusively due to heat injection as demonstrated by Simon et al. (2022).

For losing streams, downward water fluxes controlling advective heat transport lead to the depth propagation of diurnal fluctuations (Constantz, 2008). In such cases, as illustrated in Figure 2, the temperature signal recorded in the streambed (Figure 2d) is expected to be a combination of the induced temperature variations (Figure 2a) resulting from the artificial heat injection and the ambient (or natural) temperature variations due to stream water infiltration (Figure 2c). Since heating periods can require several hours or more to reduce uncertainties in flux estimates, both temperature variations (induced and ambient) may occur during heating. Therefore, for Active-DTS conducted in losing conditions, estimating water fluxes requires processing the raw temperature signal recorded to filter and remove ambient temperature variations resulting from the propagation of stream temperature fluctuations.

The temperature signal recorded at a certain depth in streambed sediments displays a phase shift and an amplitude difference compared to stream water temperature signal (Constantz, 2008). The analytical models used for modeling stream temperature propagation into streambed sediments (Anderson, 2005; Constantz, 2008; Goto et al., 2005; Hatch et al., 2006; Stallman, 1965) could have been used to model the natural temperature signal at the FO cable depth. However, these analytical models rely on the values of the thermal conductivity of sediments and the downward water flux to model the temperature signal at a certain depth. As these values are unknown at this point of the data processing, it is not possible to use them to filter data recorded during heating periods. Consequently, we developed a new methodology to process raw temperature signals.

The new approach uses temperature measurements collected along FO cables located outside heated sections to filter ambient temperature variations from raw temperature signals measured within heated FO sections. The principle consists of finding, for each measurement point located within heated sections, a "matching" measurement point located outside heated sections which experienced similar ambient temperature variations during the non heating periods. The illustrative example presented in Figure 3 shows the approach applied to temperature signal recorded in one measurement point located in a heated section. The first step consists of delimiting reference periods (Ref) corresponding to periods during which only ambient temperature variations are recorded (outside heating (H) and recovery stages). Note that, although it is reasonable to consider that heating and recovery stages have equal durations, we added 30 min to the recovery as a precaution. Then, an automated routine is used to calculate Root-Mean-Square Errors (RMSEs) between the measured temperature recorded during reference periods (red bars) and the temperature recorded for the same period outside heated sections (gray bars). We use the lowest RMSE value to associate each measurement point recorded within the heated section with a

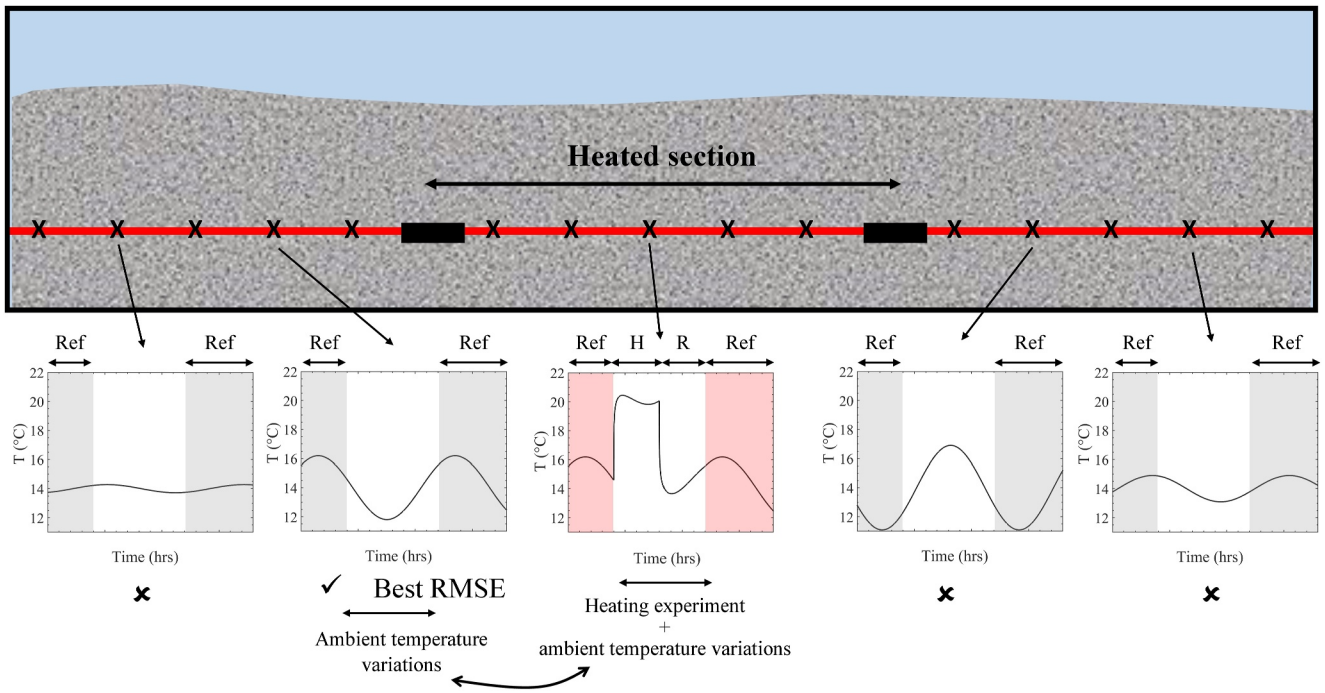

Figure 3. The principle of the method used to process temperature variations recorded along heated sections and remove ambient temperature variations, which occur predominantly in losing streams, due to the propagation of stream temperature variations in depth.

point located outside the heated sections. Then, the parameters controlling the ambient temperature variations (thermal conductivity of sediments, the downward water flux, stream temperature and the depth of the FO cable) are assumed to be identical for the heated and non-heated measurements, or at least that the combination of these parameters lead to similar ambient temperature variations. Thus, the temperature signal recorded during heating and recovery periods at the non-heated point is removed from the signal recorded at the heated point to isolate the thermal response to the artificial heat injection. This routine was applied to each measurement point location in the heated sections of the FO cable.

4. Results

4.1. Data Pre-Processing

The first step of data pre-processing consisted of removing data from non-buried sections of cable from raw temperature profiles. These were only located along F1-3/F1-2 and along F2-2/F2-1, where non-buried points represent 20% and 36% of the points collected respectively. The locations of non-buried sections found through the data analysis agrees with sections georeferenced during the installation of the cables. The second step consisted of verifying the consistency of temperature measurements. Along the section F2-4/F2-3, 62% of temperature measurement can be considered as non-representative, which means that the scale of temperature changes is certainly smaller than the spatial resolution of the DTS unit. Along other sections, temperature profiles are relatively uniform in space and only few points (<26%) are considered as "non representative." Table S1, provided as Supporting Information S1, summarizes results of data pre-processing for each heated section.

4.2. Removal of Ambient Temperature Variations

Figure 4 shows an example of data processing following the new method described in Section 3.3. The blue curves show examples of raw temperature signals recorded along heated sections and the red curves correspond to the temperature variations at a point outside the heated section which show the lowest RMSE. The black lines correspond to the processed temperature signal, once ambient temperature variations (red lines) were removed from raw temperature signal (blue lines).

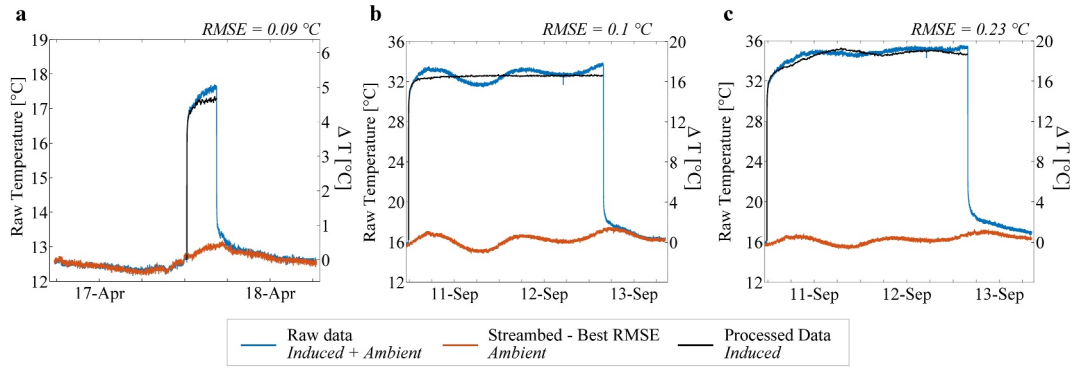

Figure 4. The data processing associates ambient temperature variations (red lines) with raw temperature signals (blue lines) to isolate the induced temperature variations (black lines), resulting from the heat injection. The three examples come from single measurement points collected (a) along the section F1-3/F1-2 (6.93 $W.m^{-1}$) in September 2018 (b) along the section F1-3/F1-1 (24.96 $W.m^{-1}$) in September 2019 (c) along the section F1-3/F1-1 (24.96 $W.m^{-1}$) in September 2019.

While the data processing is efficient (Figures 4a and 4b), the RMSEs between the heated measurement point and its associated measurement point located outside the heated section are low (≤0.1°C). In these cases, the processed temperature signal (black lines) is smooth and periodic variations induced by stream temperature variations are removed. The efficiency of the data processing is particularly obvious when heating periods are longer than 8 hr as in Figure 4b. For shorter heating periods (Figure 4a), it appears that ambient temperature variations can still impact the temperature signal (see the difference between the blue and black lines) and thus lead to a potentially large difference in the flux estimate. For instance, the interpretation of the blue curve of Figure 4a (raw temperature signal) leads to estimate $q \approx 8 \times 10^{-6}$ $m.s^{-1}$ while after data processing $q \approx 1 \times 10^{-5}$ $m.s^{-1}$, that is, a difference of 20% on flux estimate.

For larger values of RMSE (Figure 4c), the data processing may not be productive as the resulting temperature signal (black lines) can show abnormal temperature variations. For such examples, it is not possible to define a matching point in non-heated sections that shows similar ambient temperature variations. In practice, it appears that for RMSE greater than 0.2°C, measurement points could not be considered and should be removed from the data set. Despite this limitation, the number of discarded data points was negligible (less than six percent for this study). Table S1 in Supporting Information S1 provides further details on data that could not be reliability filtered.

4.3. Hyporheic Flow Estimates

4.3.1. Example of Data Interpretation

Figure 5 shows an example of data interpretation for flow estimates. Figure 5 corresponds to the normalized temperature profiles (ΔT/Q) obtained along the heated sections of the cable FO1 after 4 hr of heat injection. These data correspond to those processed as described previously (293 measurements points). The gaps correspond to location of measurement points that were not interpreted because of non-buried sections, small-scale temperature gradient or the difficulty in removing ambient temperature variations. It is worth noting that these points are generally grouped over a few meters sections and not isolated in space (see Figures 6 and 8). Thus, although some sections are not interpreted, the method provides an excellent overview of the variability at high spatial resolution of water fluxes along the 120 m stream reach.

The ADTS Toolbox (Simon & Bour, 2023) was used to interpret evolution curves and to estimate groundwater flux and thermal conductivity. Figure 5 shows several examples of interpreted thermal response curves. Along the heated section, some measurement points show similar temperature increases (a_1 and a_2), which reflect similar values of thermal conductivities and water fluxes (Figure 5b). Other locations show similar temperature evolution during the conduction-dominant period but show different temperature stabilizations for later time, during the advection-dominant period (b_1, b_2 and b_2). These points are therefore characterized by similar thermal conductivities, but different groundwater fluxes (Figure 5c). Results also show that measurement points (c_1 and c_2) can be characterized in terms of different thermal conductivities and similar groundwater fluxes. The ADTS Toolbox can further efficiently reproduce the measured temperature increases (Figures 5b–5d).

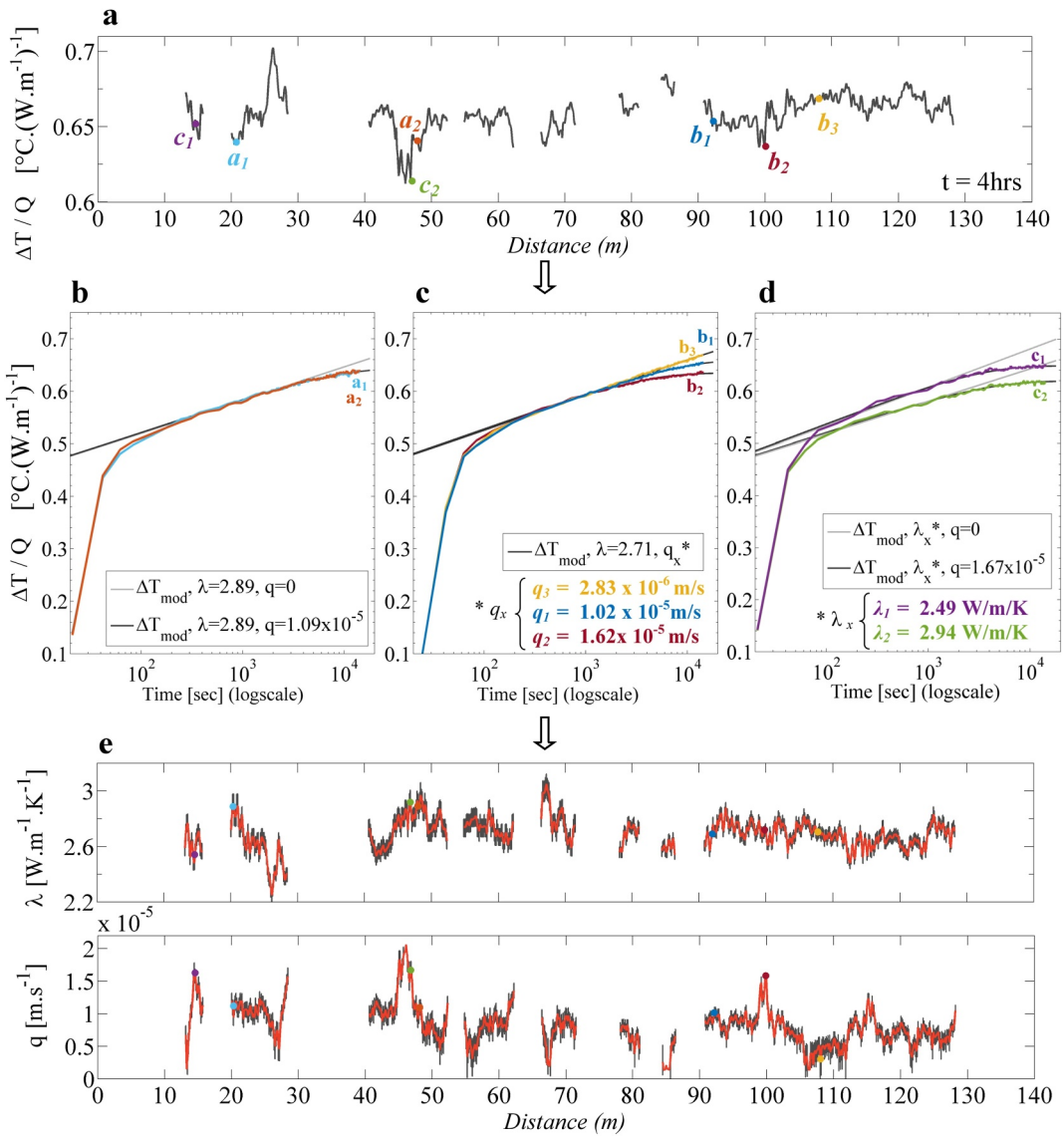

Figure 5. Interpretation of temperature elevations measured along section FO1 in April 2018 (F1-3/F1-2 heated at 20.12 W.m^{-1} and F1-2/F1-1 heated at 30.13 W.m^{-1}). (a) Normalized temperature profiles (ΔT/Q) obtained four hours after start of heating. Q is the constant linear heating power [W.m^{-1}] (b–d) Examples of temperature increase recorded along heated sections. Indexes (a_1, a_2 etc.) refer to the location of each measurement point along the profile (a). (e) Profiles of thermal conductivities (above) and of water fluxes (below) estimated from temperature elevations and interpreted through the ADTS toolbox. Gray bars represent uncertainties.

Having interpreted each measurement point, we obtain the profiles of thermal conductivities and water fluxes (Figure 5e). The uncertainty on estimates is calculated considering the data noise of the temperature signal as the dominant influence (Simon & Bour, 2023).

4.3.2. Spatial Variability

Figure 6 shows profiles of thermal conductivities (a) and of water fluxes (b) as a function of distance along the cable. Thermal conductivities of sediments vary between 2.1 and 2.9 W.m^{-1}.K^{-1}, with an uncertainty regarding the data interpretation on estimates of 0.1 W.m^{-1}.K^{-1}. This result is consistent with values of thermal conductivity commonly measured in saturated sand, that is, 1.5–4.0 W.m^{-1}.K^{-1} (Stauffer et al., 2013).

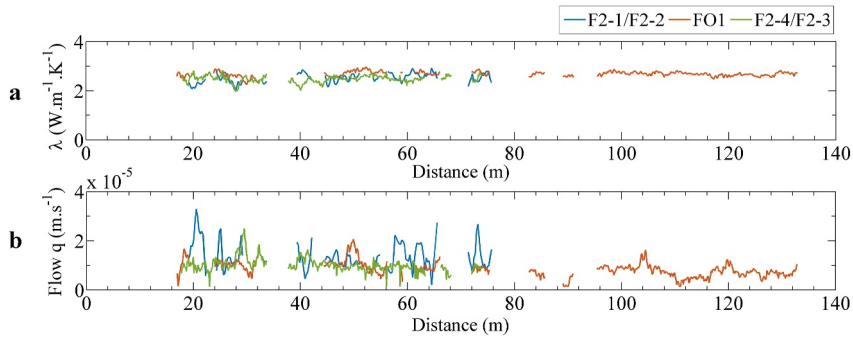

Figure 6. Profiles of thermal conductivities (a) and of water fluxes (b) obtained from Active-DTS measurements conducted in April 2018 along F2-1/F2-2 (blue line), FO1 including F1-1/F1-2, and F1-2/F1-3 (orange line), and F2-4/F2-3 (green line).

Downward water fluxes along each of the three sections vary between 5×10^{-6} and 3.5×-10^{-5} m.s^{-1}, with an uncertainty <10%. The mean water flux for all sections is 9.7×-10^{-6} m.s^{-1} and the standard deviation 3.8×10^{-6} m.s^{-1}.

Figure 7 shows the distributions of thermal conductivities (a-d) and of water fluxes (e-h) obtained for each heated section. Based on Kolmogorov-Smirnov tests, the values of estimated thermal conductivities follow normal distributions (red curves) with similar means (2.47–2.69 W.m^{-1}.K^{-1}) and small values of standard deviations (<0.2 W.m^{-1}.K^{-1}). Kolmogorov-Smirnov tests also show that the values of fluxes estimated along F1-2/F1-1 (Figure 7h) also follow normal distributions. Along other sections, the values of estimated water fluxes are tightly distributed with relatively small values of standard deviations (between 2.9×10^{-6} and 5.5×10^{-6}m.s^{-1}), but are not statistically normally distributed. This is not surprising since water flux estimates are more variable along this latter section (see blue line in Figure 6b). Note that no clear correlation appears between the profiles of downward water flux estimated and the streambed topography profile (see Figure S4 in Supporting Information S1). This suggests that water flux variations do not depend here on the streambed topography.

GPS measurements made along the FO cable facilitate the spatial mapping of hyporheic flow across the stream at the study site (Figure 8). Despite the small values of standard deviation of water fluxes estimated, water fluxes seem to be slightly higher in the middle of the stream. This was confirmed by a Mood's median test, which highlighted that water fluxes along these two sections are statistically distinct (p-value < 0.001 with an observed critical value of 62.86, higher than the critical value = 3.84).

4.3.3. Temporal Variability

Figure 9 shows thermal conductivities (a) and water fluxes (b,c,d) estimated along the cable FO1 at different times. Despite the different hydrological conditions, the estimates of thermal conductivity and the estimates water flux estimates vary little over time. Nevertheless, water fluxes appear slightly lower when estimated during the last field campaign in September 2019, specifically along the section between 0 and 70 m. Apart from this outlier, the data show remarkable reproducibility, with excellent accuracy in determining thermal conductivities and water fluxes.

5. Discussion

5.1. Applicability and Limitations of the Method

In this study, we demonstrated the feasibility of performing Active-DTS in the hyporheic zone of a large lowland river. Despite some difficulties in burying the FO cables, sediment thermal conductivities and hyporheic flows were successfully estimated along large, continuous sections of the river. This highlights the primary advantage of the method, as existing methods (i.e., seepage meters, VTPs, etc.) are unable to make such estimates with similar spatial resolution. Moreover, by providing water flux estimates with low uncertainties, the approach provides higher quality data than conventional methods dependent on hydraulic conductivity estimates. The measurements collected over varying sampling periods within the same spatial bounds show excellent reproducibility, confirming the accuracy of the method.

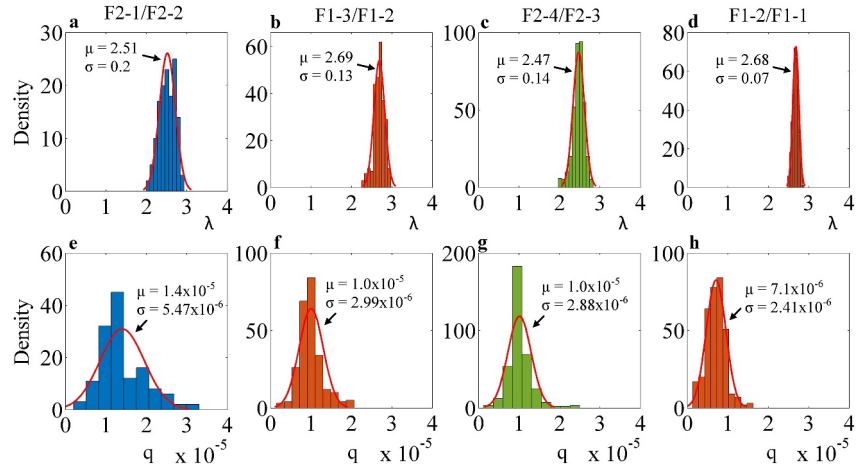

Figure 7. (a–d) Distributions of thermal conductivities λ [$W.m^{-1}.K^{-1}$] estimated for each heated section. (e–h) Distributions of water fluxes q [$m.s^{-1}$] estimated for each heated section. Red curves correspond to normal distributions fitted to the estimates with associated mean values (μ).

This study also highlights the utility of Active-DTS methods in a losing river environment. We have shown how to efficiently remove ambient temperature variation from the majority of raw data. The method presented here to filter ambient temperature variations could also be useful in gaining streams, since stream temperature may also propagate with depth when upward fluxes are small. The data filtering relies on identifying two measurement points displaying similar ambient temperature variations, which may be difficult in highly heterogeneous conditions. In this case, monitoring temperature along longer non-heated sections should increase the probability of finding a matching point.

The deployment of the FO cable in large streams is challenging due to high stream water levels preventing the burial of the FO cable. Here, the use of a plow solved that problem and ensured the cable depth was relatively consistent. This also helped to protect the streambed, which is important since burying a cable in a streambed may impact sensitive ecosystems. To illustrate that the plow limits the destruction of the streambed, a movie showing the cable installation within the streambed is provided as Supporting Information S1. However, even with the use

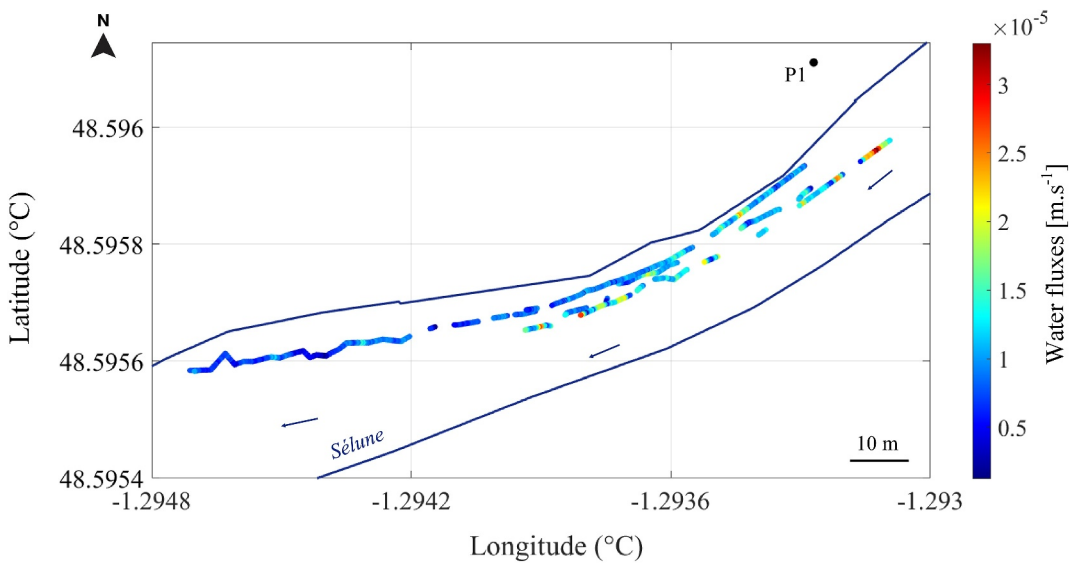

Figure 8. Map of hyporheic fluxes estimated along heated FO cables (April 2018). The blue curves correspond to the banks of the Sélune river.

10.1029/2023WR035475

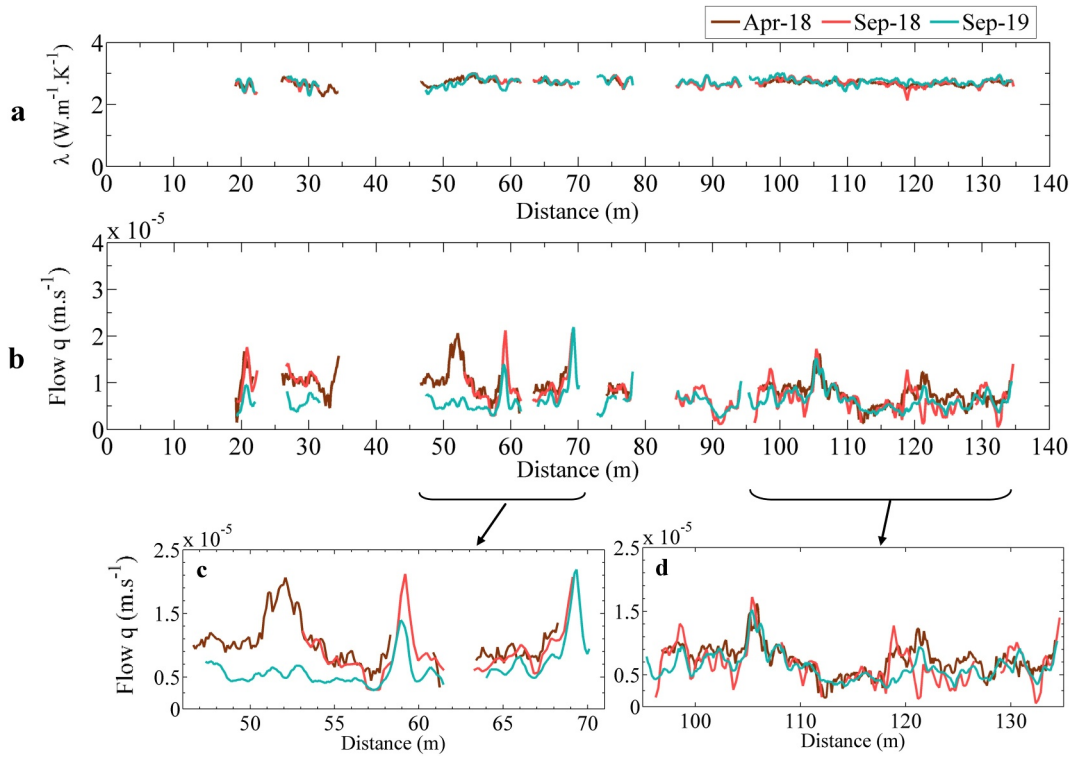

Figure 9. Profiles of thermal conductivities (a) and of water fluxes (b) obtained along the FO1 from Active-DTS measurements conducted in April 2018 (brown lines), in September 2018 (pink lines) and in September 2019 (green lines). Plots (c) and (d) are zoomed sections of profiles shown in (b).

of the plow, it was not possible to bury the FO cable everywhere because of impenetrable streambed substrate areas. Likewise, even if the cable burial was controlled during the installation, the burial depth may slightly vary in space. This is not critical as the data interpretation does not depend on burial depth. However, if the burial depth of the cable is less than 3 cm, the induced heat is expected to be partly dissipated in the stream, which would affect the temperature increase. In our study, the burial depth of the cable seems acceptable since significant temperature increases were recorded along the heated sections. Once installed, the armored FO cable can remain in the river without being impacted. This allowed long-term monitoring for different hydrological conditions or for variations in streambed properties caused by clogging for instance. At Signy, the streambed is stable, and then burying the FO cable at 10 cm-depth is enough. However, if the geometry and the geomorphology of the stream change rapidly, as observed for instance in braided rivers, the burial depth of the cable may become an issue.

The main limitation of the method is the inability to determine the flux direction. Here, measurements were performed in a predominantly losing river section. Pumping in the aquifer close to the stream induces a significant hydraulic gradient between the stream and the aquifer with permanent losing conditions. Because of this, it is assumed that fluxes are mainly downward and that the flow paths in the hyporheic zone are simple, in comparison to natural flow conditions. This means that a 1D heat model is sufficient for data interpretation. In the case of natural flow conditions, the flow paths in the hyporheic may be more complex, meaning that complementary methods, such as seepage meters (Humphrey et al., 2022; Rosenberry et al., 2020) or heat-pulse probes (Banks et al., 2018; Lewandowski et al., 2011; Zlotnik & Tartakovsky, 2018), should be used to characterize flow direction. Indeed, studies assessing the effect of non-perpendicular fluxes on the thermal response suggest that the magnitude of temperature increase is significantly affected as soon as the angle between the fiber-optic cable and the water flux is less than 60° (at 90° the cable and the flow being orthogonal) (Aufleger et al., 2007; Chen et al., 2019; Perzlmaier et al., 2004). In natural conditions (no pumping), this assumption may not be fulfilled since local streambed topography may induce complex flowpaths within the hyporheic zone (Tonina & Buffington, 2011).

5.2. Spatial Variability of Fluxes

Perhaps surprisingly, our results show that thermal conductivities and water fluxes are relatively homogeneous along or across the streambed sediments. As shown by their distribution (Figure 7), water fluxes vary over less than an order of magnitude with a mean value around 1×10^{-5} m.s^{-1}. At Signy, the mean hydraulic gradient between the stream level and the groundwater level at pumping boreholes is around 8–9 $\times 10^{-3}$ m.m^{-1}, which implies that the hydraulic conductivity is around 1.2×10^{-3} m.s^{-1}. This is in good agreement with values commonly encountered in sand (10^{-3}–10^{-5} m.s^{-1}) and gravel (10^{-2}–10^{-3} m.s^{-1}) materials (Shackelford, 2013), which shows the consistency of flux measurements. The high value of hydraulic conductivity is also consistent with a rapid groundwater response to stream stage variations observed. In contrast, Simon et al. (2022) found larger ranges of water fluxes and thermal conductivities at the stream-groundwater interface in a headwater stream, with thermal conductivities varying between 0.8 and 3.14 W.m^{-1}.K^{-1} and fluxes varying between 2×10^{-4} and 5×10^{-5} m.s^{-1}.

Our experimental setup allows for high resolution mapping of both the longitudinal and lateral variability of water flux, which is a major advance (Figure 8). Most of the data suggest stream water infiltration is slightly higher in the middle of the river than close to the riverbank. This could have an effect on the thermal stratigraphy or on biogeochemical processus in this section of the river, but this result warrants further investigation. Regardless, the flux variability remains small. It may be that the low variability is due to the data processing, which removed a significant percentage of the data (between 24% and 65% depending on the section) before the interpretation. However, as shown in Figures 6a and 8, there are several long sections of cables (up to almost 40 m length) where data are continuous in space. This suggests that thermal conductivities and hyporheic fluxes are truly homogeneous at such scale, which is a significant conclusion for describing the properties of the hyporheic zone.

The spatial variability of hyporheic flow is potentially due to heterogeneities induced by streambed hydraulic conductivity and/or to streambed topography variations inducing differences in hydraulic gradients. When the stream water level varies by 0.4 m, consistent with streambed topographic variations, the hydraulic gradient, and therefore water fluxes, should vary by 10%–15%. Variations of this scale should be detectable given the sensitivity of the method, implying that, streambed topography variations should partly control hyporheic flow. However, results do not show a clear correlation between water flux distribution and the bedform topography (Figure S4 in Supporting Information S1). In practice, the significant hydraulic gradient imposed by pumping is probably larger than the potential effect of streambed topography variations on flow paths. Consequently, the water flux variability in the streambed is likely to be controlled by local geological heterogeneities. This means that, in our case, the water flux variability may be used as an indicator of hydraulic conductivity variability. By considering a uniform average hydraulic gradient along the profile and as water fluxes vary over one order of magnitude it can be inferred that hydraulic conductivities also vary within one order of magnitude. This result could help in calibrating hydrological models, in which hydraulic conductivity is generally assumed.

This approach could provide hydraulic conductivities with high spatial resolution and the added benefit of low uncertainties. However, under natural conditions, without any pumping in the alluvial aquifer, the effect of streambed topography variations may be more important. In this case, both streambed variations and heterogeneities would control hyporheic flow variations and direction and it would be more difficult to make reliable inference about streambed heterogeneities. However, if streambed topography is well-characterized, with airborne LiDAR for instance (Lague & Feldmann, 2020), as well as the local hydraulic gradients within the streambed (Cucchi et al., 2018), it would be possible to clearly identify the impact of both effects.

5.3. Temporal Variability of Fluxes

Despite temporal variations in groundwater levels measured at the field site, water infiltration in the riverbed was nearly constant over time. This can be explained by the high permeability of the stream bed. The recording of temporal variations in stream level and in hydraulic head in the sediments shows that the local hydraulic head is quasi-constant over time. Likewise, on a larger scale, the hydraulic gradient between the stream and the wells used for water supply changed less than eight percent between 2017 and 2020 at the site. This suggests that the hyporheic flow is mainly controlled by the large-scale hydraulic gradient imposed by groundwater pumping for local water supply. Therefore, hyporheic flows seem to remain mostly stable over time. In other hydrogeological conditions, Active-DTS experiments could be very well suited for monitoring hyporheic fluxes variations at different time scales. The method could be used to monitor the seasonal variability of water fluxes by repeating

the surveys under different hydrological conditions. It could also be used for assessing diurnal variations of fluxes, because of evapotranspiration, or the effect of rainfall/flooding events on hyporheic fluxes (Simon, Bour, Lavenant, et al., 2023).

Another interesting observation is that between 20 and 35m and between 45 and 62 m along FO1 (Figures 9b and 9c), calculated water fluxes in September 2019 are less than half the calculated fluxes during other periods (while thermal conductivities estimates are similar). This change in flow over time may be due to a decrease of hydraulic conductivity of the streambed, due to local clogging, itself likely caused by the removal of the Vezin dam, a few kilometers upstream. This dam was destroyed in spring 2019 and this leads to a large increase in the river turbidity. Variations in hydraulic conductivity of this magnitude commonly result from erosion and deposition processes (Gianni et al., 2016). However, it should be noted that no temporal changes of water fluxes were observed along the FO2 cable showing that, if clogging occurred, it only affected a part of the river. Note also that such variations with time could also be due to local deposition of sediments that may induce some changes in groundwater fluxes, but this point goes beyond the scope of our study.

6. Conclusions

Active-DTS measurements were conducted along a 120 m reach of a lowland river to demonstrate the feasibility of our method to characterize and map the spatiotemporal variability of fluxes in the hyporheic zone. The DTS technology provides profound spatiotemporal insights, well beyond the fluxes provided by any other method. The approach provided estimates of thermal conductivities and water fluxes along the two FO cables buried within the streambed sediments at a depth of 10 cm. Repeating surveys in 2018 and 2019, under different hydrological conditions provided an assessment of the change in flux with time and their temporal variabilities. The ability to quantify and monitor water fluxes within the hyporheic zone at high resolution and with low uncertainties is an important outcome for characterizing flow in the hyporheic zone.

Our results show that thermal conductivities and water fluxes present minor variations in space and in time for our study site and river setting. Due to pumping in the alluvial aquifer near the stream, the absence of a clear relationship between water flux variations and streambed topography suggests that the observed spatial variability of hyporheic flow is primarily due to streambed heterogeneities. Therefore, in this case, an advantage of the approach is that the variability of water fluxes can be considered here as an indicator of heterogeneity within the streambed. Thus, we expect the water fluxes and the hydraulic conductivities to have the similar distribution, meaning that sediment hydraulic conductivities are expected to vary only over one order of magnitude. This unique insight should serve to improve understanding of flow paths in the hyporheic zone. Further, our novel deployment enhances the spatial resolution applied to characterizing stream bed heterogeneities. Furthermore, in most sections, the thermal conductivity and water flux show negligible variations over time. The measurements were found to be remarkably stable and reproducible during few years, implying that fluxes in the hyporheic zone may be stable over time at the field site.

Data Availability Statement

Data to support the findings for this research are available on "Recherche Data Gouv" (Simon, Bour, & Crave, 2023).

Acknowledgments
This work was supported by the Agence de l'Eau Loire Bretagne and by the ANR project EQUIPEX CRITEX (Grant ANR-11-EQPX-0011). We warmly thank Mamadou Ndom for his support during the installation of the FO cable, as well as Kerry Gallagher for English corrections and his kind and insightful suggestions. We also sincerely thank the associate editor, Prof. Dr. Jan Fleckenstein, and three reviewers for their remarks and comments that greatly help to improve the manuscript.

References

Anderson, M. P. (2005). Heat as a ground water tracer. *Ground Water*, *43*(6), 951–968. https://doi.org/10.1111/j.1745-6584.2005.00052.x

Arnon, S., Marx, L. P., Searcy, K. E., & Packman, A. I. (2010). Effects of overlying velocity, particle size, and biofilm growth on stream–subsurface exchange of particles. *Hydrological Processes*, *24*(1), 108–114. https://doi.org/10.1002/hyp.7490

Aufleger, M., Conrad, M., Goltz, M., Perzlmaier, S., & Porras, P. (2007). Innovative dam monitoring tools based on distributed temperature measurement. *Jordan Journal of Civil Engineering*, *1*, 29–37.

Banks, E. W., Morgan, L. K., Sai Louie, A. J., Dempsey, D., & Wilson, S. R. (2022). Active distributed temperature sensing to assess surface water–groundwater interaction and river loss in braided river systems. *Journal of Hydrology*, *615*, 128667. https://doi.org/10.1016/j.jhydrol.2022.128667

Banks, E. W., Shanafield, M. A., Noorduijn, S., McCallum, J., Lewandowski, J., & Batelaan, O. (2018). Active heat pulse sensing of 3-D-flow fields in streambeds. *Hydrology and Earth System Sciences*, *22*(3), 1917–1929. https://doi.org/10.5194/hess-22-1917-2018

Bardini, L., Boano, F., Cardenas, M. B., Sawyer, A. H., Revelli, R., & Ridolfi, L. (2013). Small-scale permeability heterogeneity has negligible effects on nutrient cycling in streambeds. *Geophysical Research Letters*, *40*(6), 1118–1122. https://doi.org/10.1002/grl.50224

Bencala, K. (1993). A perspective on stream-catchment connections. *Journal of the North American Benthological Society*, *12*(1), 44–47. https://doi.org/10.2307/1467684

Bense, V. F., Read, T., Bour, O., Le Borgne, T., Coleman, T., Krause, S., et al. (2016). Distributed temperature sensing as a downhole tool in hydrogeology. *Water Resources Research*, *52*(12), 9259–9273. https://doi.org/10.1002/2016WR018869

Boano, F., Camporeale, C., & Revelli, R. (2010). A linear model for the coupled surface-subsurface flow in a meandering stream. *Water Resources Research*, *46*(7), W07535. https://doi.org/10.1029/2009WR008317

Boano, F., Camporeale, C., Revelli, R., & Ridolfi, L. (2006). Sinuosity-driven hyporheic exchange in meandering rivers. *Geophysical Research Letters*, *33*(18), L18406. https://doi.org/10.1029/2006GL027630

Boano, F., Harvey, J. W., Marion, A., Packman, A. I., Revelli, R., Ridolfi, L., & Wörman, A. (2014). Hyporheic flow and transport processes: Mechanisms, models, and biogeochemical implications. *Reviews of Geophysics*, *52*(4), 603–679. https://doi.org/10.1002/2012RG000417

Boano, F., Revelli, R., & Ridolfi, L. (2007). Bedform-induced hyporheic exchange with unsteady flows. *Advances in Water Resources*, *30*(1), 148–156. https://doi.org/10.1016/j.advwatres.2006.03.004

Briggs, M. A., Buckley, S. F., Bagtzoglou, A. C., Werkema, D. D., & Lane, J. W. (2016). Actively heated high-resolution fiber-optic-distributed temperature sensing to quantify streambed flow dynamics in zones of strong groundwater upwelling. *Water Resources Research*, *52*(7), 5179–5194. https://doi.org/10.1002/2015WR018219

Brunner, P., Therrien, R., Renard, P., Simmons, C. T., & Franssen, H.-J. H. (2017). Advances in understanding river-groundwater interactions. *Reviews of Geophysics*, *55*(3), 818–854. https://doi.org/10.1002/2017RG000556

Cardenas, M. B. (2008a). Surface water-groundwater interface geomorphology leads to scaling of residence times. *Geophysical Research Letters*, *35*(8), L08402. https://doi.org/10.1029/2008GL033753

Cardenas, M. B. (2008b). The effect of river bend morphology on flow and timescales of surface water–groundwater exchange across pointbars. *Journal of Hydrology*, *362*(1), 134–141. https://doi.org/10.1016/j.jhydrol.2008.08.018

Cardenas, M. B. (2009). A model for lateral hyporheic flow based on valley slope and channel sinuosity. *Water Resources Research*, *45*(1), W01501. https://doi.org/10.1029/2008WR007442

Cardenas, M. B., & Wilson, J. L. (2007). Dunes, turbulent eddies, and interfacial exchange with permeable sediments. *Water Resources Research*, *43*(8), W08412. https://doi.org/10.1029/2006WR005787

Cardenas, M. B., Wilson, J. L., & Zlotnik, V. A. (2004). Impact of heterogeneity, bed forms, and stream curvature on subchannel hyporheic exchange. *Water Resources Research*, *40*(8), W08307. https://doi.org/10.1029/2004WR003008

Carslaw, H. S., & Jaeger, J. C. (1959). *Conduction of heat in solids*. Oxford Univers. Press. Retrieved from https://infoscience.epfl.ch/record/27427

Chen, J., Xiong, F., Zheng, J., Ge, Q., & Cheng, F. (2019). The influence of infiltration angle on the identification effect of seepage with linear heat source method. *Measurement*, *148*, 106974. https://doi.org/10.1016/j.measurement.2019.106974

Constantz, J. (2008). Heat as a tracer to determine streambed water exchanges. *Water Resources Research*, *44*(4), W00D10. https://doi.org/10.1029/2008WR006996

Cucchi, K., Rivière, A., Baudin, A., Berrhouma, A., Durand, V., Rejiba, F., et al. (2018). LOMOS-mini: A coupled system quantifying transient water and heat exchanges in streambeds. *Journal of Hydrology*, *561*, 1037–1047. https://doi.org/10.1016/j.jhydrol.2017.10.074

del Val, L., Carrera, J., Pool, M., Martínez, L., Casanovas, C., Bour, O., & Folch, A. (2021). Heat dissipation test with fiber-optic distributed temperature sensing to estimate groundwater flux. *Water Resources Research*, *57*(3), e2020WR027228. https://doi.org/10.1029/2020WR027228

des Tombe, B. F., Bakker, M., Smits, F., Schaars, F., & van der Made, K.-J. (2019). Estimation of the variation in specific discharge over large depth using distributed temperature sensing (DTS) Measurements of the heat pulse response. *Water Resources Research*, *55*(1), 811–826. https://doi.org/10.1029/2018WR024171

Diao, N., Li, Q., & Fang, Z. (2004). Heat transfer in ground heat exchangers with groundwater advection. *International Journal of Thermal Sciences*, *43*(12), 1203–1211. https://doi.org/10.1016/j.ijthermalsci.2004.04.009

Fleckenstein, J. H., Krause, S., Hannah, D. M., & Boano, F. (2010). Groundwater-surface water interactions: New methods and models to improve understanding of processes and dynamics. *Special Issue on ground water-surface water interactions*, *33*(11), 1291–1295. https://doi.org/10.1016/j.advwatres.2010.09.011

Flipo, N., Monteil, C., Poulin, M., de Fouquet, C., & Krimissa, M. (2012). Hybrid fitting of a hydrosystem model: Long-term insight into the Beauce aquifer functioning (France). *Water Resources Research*, *48*(5), W05509. https://doi.org/10.1029/2011WR011092

Flipo, N., Mouhri, A., Labarthe, B., Biancamaria, S., Rivière, A., & Weill, P. (2014). Continental hydrosystem modelling: The concept of nested stream-aquifer interfaces. *Hydrology and Earth System Sciences*, *18*(8), 3121–3149. https://doi.org/10.5194/hess-18-3121-2014

Fovet, O., Ndom, M., Crave, A., & Pannard, A. (2020). Influence of dams on river water-quality signatures at event and seasonal scales: The Sélune River (France) case study. *River Research and Applications*, *36*(7), 1267–1278. https://doi.org/10.1002/rra.3618

Fox, A., Boano, F., & Arnon, S. (2014). Impact of losing and gaining streamflow conditions on hyporheic exchange fluxes induced by dune-shaped bed forms. *Water Resources Research*, *50*(3), 1895–1907. https://doi.org/10.1002/2013WR014668

Fox, A., Laube, G., Schmidt, C., Fleckenstein, J. H., & Arnon, S. (2016). The effect of losing and gaining flow conditions on hyporheic exchange in heterogeneous streambeds. *Water Resources Research*, *52*(9), 7460–7477. https://doi.org/10.1002/2016WR018677

Frei, S., Durejka, S., Le Lay, H., Thomas, Z., & Gilfedder, B. S. (2019). Quantification of hyporheic nitrate removal at the reach scale: Exposure times versus residence times. *Water Resources Research*, *55*(11), 9808–9825. https://doi.org/10.1029/2019WR025540

Genereux, D. P., Leahy, S., Mitasova, H., Kennedy, C. D., & Corbett, D. R. (2008). Spatial and temporal variability of streambed hydraulic conductivity in West Bear Creek, North Carolina, USA. *Journal of Hydrology*, *358*(3), 332–353. https://doi.org/10.1016/j.jhydrol.2008.06.017

Gianni, G., Richon, J., Perrochet, P., Vogel, A., & Brunner, P. (2016). Rapid identification of transience in streambed conductance by inversion of floodwave responses. *Water Resources Research*, *52*(4), 2647–2658. https://doi.org/10.1002/2015WR017154

Gomez-Velez, J. D., & Harvey, J. W. (2014). A hydrogeomorphic river network model predicts where and why hyporheic exchange is important in large basins. *Geophysical Research Letters*, *41*(18), 6403–6412. https://doi.org/10.1002/2014GL061099

Goto, S., Yamano, M., & Kinoshita, M. (2005). Thermal response of sediment with vertical fluid flow to periodic temperature variation at the surface. *Journal of Geophysical Research*, *110*(B1), B01106. https://doi.org/10.1029/2004JB003419

Harvey, J., & Bencala, K. (1993). The effect of streambed topography on surface-subsurface water exchange. *Water Resources Research*, *29*(1), 89–98. https://doi.org/10.1029/92WR01960

Hatch, C. E., Fisher, A. T., Revenaugh, J. S., Constantz, J., & Ruehl, C. (2006). Quantifying surface water-groundwater interactions using time series analysis of streambed thermal records: Method development. *Water Resources Research*, *42*(10), W10410. https://doi.org/10.1029/2005WR004787

Hermans, T., Goderniaux, P., Jougnot, D., Fleckenstein, J. H., Brunner, P., Nguyen, F., et al. (2023). Advancing measurements and representations of subsurface heterogeneity and dynamic processes: Towards 4D hydrogeology. *Hydrology and Earth System Sciences*, *27*(1), 255–287. https://doi.org/10.5194/hess-27-255-2023

Hester, E. T., Cardenas, M. B., Haggerty, R., & Apte, S. V. (2017). The importance and challenge of hyporheic mixing. *Water Resources Research*, *53*(5), 3565–3575. https://doi.org/10.1002/2016WR020005

Hester, E. T., Eastes, L. A., & Widdowson, M. A. (2019). Effect of surface water stage fluctuation on mixing-dependent hyporheic denitrification in riverbed dunes. *Water Resources Research*, *55*(6), 4668–4687. https://doi.org/10.1029/2018WR024198

Humphrey, C. E., Solomon, D. K., Genereux, D. P., Gilmore, T. E., Mittelstet, A. R., Zlotnik, V. A., et al. (2022). Using automated seepage meters to quantify the spatial variability and net flux of groundwater to a stream. *Water Resources Research*, *58*(6), e2021WR030711. https://doi.org/10.1029/2021WR030711

Jones, J. B., & Mulholland, P. J. (2000). Aquatic ecology series. In *Streams and ground waters* (p. II). Academic Press. https://doi.org/10.1016/B978-0-12-389845-6.50020-X

Kalbus, E., Reinstorf, F., & Schirmer, M. (2006). Measuring methods for groundwater - Surface water interactions: A review. *Hydrology and Earth System Sciences*, *10*(6), 873–887. https://doi.org/10.5194/hess-10-873-2006

Kaufman, M. H., Cardenas, M. B., Buttles, J., Kessler, A. J., & Cook, P. L. M. (2017). Hyporheic hot moments: Dissolved oxygen dynamics in the hyporheic zone in response to surface flow perturbations. *Water Resources Research*, *53*(8), 6642–6662. https://doi.org/10.1002/2016WR020296

Krause, S., Abbott, B. W., Baranov, V., Bernal, S., Blaen, P., Datry, T., et al. (2022). Organizational principles of hyporheic exchange flow and biogeochemical cycling in river networks across scales. *Water Resources Research*, *58*(3), e2021WR029771. https://doi.org/10.1029/2021WR029771

Krause, S., Hannah, D. M., & Fleckenstein, J. H. (2009). Hyporheic hydrology: Interactions at the groundwater-surface water interface. *Hydrological Processes*, *23*(15), 2103–2107. https://doi.org/10.1002/hyp.7366

Krause, S., Hannah, D. M., Fleckenstein, J. H., Heppell, C. M., Kaeser, D., Pickup, R., et al. (2011). Inter-disciplinary perspectives on processes in the hyporheic zone. *Ecohydrology*, *4*(4), 481–499. https://doi.org/10.1002/eco.176

Kurth, A.-M., Weber, C., & Schirmer, M. (2015). How effective is river restoration in re-establishing groundwater-surface water interactions? - A case study. *Hydrology and Earth System Sciences*, *19*(6), 2663–2672. https://doi.org/10.5194/hess-19-2663-2015

Lague, D., & Feldmann, B. (2020). Chapter 2—Topo-bathymetric airborne LiDAR for fluvial-geomorphology analysis. In P. Tarolli & S. M. Mudd (Éds.), *Developments in Earth surface processes* (Vol. 23, p. 25–54). Elsevier. https://doi.org/10.1016/B978-0-444-64177-9.00002-3

Landon, M. K., Rus, D. L., & Harvey, F. E. (2001). Comparison of instream methods for measuring hydraulic conductivity in sandy streambeds. *Groundwater*, *39*(6), 870–885. https://doi.org/10.1111/j.1745-6584.2001.tb02475.x

Laube, G., Schmidt, C., & Fleckenstein, J. H. (2018). The systematic effect of streambed conductivity heterogeneity on hyporheic flux and residence time. *Advances in Water Resources*, *122*, 60–69. https://doi.org/10.1016/j.advwatres.2018.10.003

Lewandowski, J., Angermann, L., Nuetzmann, G., & Fleckenstein, J. H. (2011). A heat pulse technique for the determination of small-scale flow directions and flow velocities in the streambed of sand-bed streams. *Hydrological Processes*, *25*(20), 3244–3255. https://doi.org/10.1002/hyp.8062

Mamer, E. A., & Lowry, C. S. (2013). Locating and quantifying spatially distributed groundwater/surface water interactions using temperature signals with paired fiber-optic cables. *Water Resources Research*, *49*(11), 7670–7680. https://doi.org/10.1002/2013WR014235

Perzlmaier, S., Aufleger, M., & Conrad, M. (2004). Distributed fiber optic temperature measurements in hydraulic engineering: Prospects of the heat-up method. In *Proceedings of a workshop on dam safety problems and solutions, 72nd ICOLD annual meeting, Seoul, South Korea*.

Read, T., Bour, O., Selker, J. S., Bense, V. F., Borgne, T. L., Hochreutener, R., & Lavenant, N. (2014). Active-distributed temperature sensing to continuously quantify vertical flow in boreholes. *Water Resources Research*, *50*(5), 3706–3713. https://doi.org/10.1002/2014WR015273

Revelli, R., Boano, F., Camporeale, C., & Ridolfi, L. (2008). Intra-meander hyporheic flow in alluvial rivers. *Water Resources Research*, *44*(12), W12428. https://doi.org/10.1029/2008WR007081

Rosenberry, D. O., Duque, C., & Lee, D. R. (2020). History and evolution of seepage meters for quantifying flow between groundwater and surface water: Part 1 – Freshwater settings. *Earth-Science Reviews*, *204*, 103167. https://doi.org/10.1016/j.earscirev.2020.103167

Salehin, M., Packman, A. I., & Paradis, M. (2004). Hyporheic exchange with heterogeneous streambeds: Laboratory experiments and modeling. *Water Resources Research*, *40*(11), W11504. https://doi.org/10.1029/2003WR002567

Schmidt, C., Bayer-Raich, M., & Schirmer, M. (2006). Characterization of spatial heterogeneity of groundwater-stream water interactions using multiple depth streambed temperature measurements at the reach scale. *Hydrology and Earth System Sciences*, *10*(6), 849–859. https://doi.org/10.5194/hess-10-849-2006

Shackelford, C. D. (2013). Geoenvironmental engineering. In *Reference module in earth systems and environmental sciences*. Elsevier. https://doi.org/10.1016/B978-0-12-409548-9.05424-5

Shanafield, M., Banks, E. W., Arkwright, J. W., & Hausner, M. B. (2018). Fiber-optic sensing for environmental applications: Where we have come from and what is possible. *Water Resources Research*, *54*(11), 8552–8557. https://doi.org/10.1029/2018WR022768

Shanafield, M., Pohll, G., & Susfalk, R. (2010). Use of heat-based vertical fluxes to approximate total flux in simple channels. *Water Resources Research*, *46*(3), W03508. https://doi.org/10.1029/2009WR007956

Simon, N., & Bour, O. (2023). An ADTS toolbox for automatically interpreting active distributed temperature sensing measurements. *Groundwater*, *61*(2), 215–223. https://doi.org/10.1111/gwat.13172

Simon, N., Bour, O., & Crave, A. (2023). Dataset of "Spatiotemporal variability of hyporheic flow in a losing river section. *Recherche Data Gouv*. https://doi.org/10.57745/FHITDV

Simon, N., Bour, O., Faucheux, M., Lavenant, N., Le Lay, H., Fovet, O., et al. (2022). Combining passive and active distributed temperature sensing measurements to locate and quantify groundwater discharge variability into a headwater stream. *Hydrology and Earth System Sciences*, *26*(5), 1459–1479. https://doi.org/10.5194/hess-26-1459-2022

Simon, N., Bour, O., Lavenant, N., Porel, G., Nauleau, B., & Klepikova, M. (2023). Monitoring groundwater fluxes variations through active-DTS measurements. *Journal of Hydrology*, *622*, 129755. https://doi.org/10.1016/j.jhydrol.2023.129755

Simon, N., Bour, O., Lavenant, N., Porel, G., Nauleau, B., Pouladi, B., & Longuevergne, L. (2020). A comparison of different methods to estimate the effective spatial resolution of FO-DTS measurements achieved during sandbox experiments. *Sensors*, *20*(2), 570. https://doi.org/10.3390/s20020570

Simon, N., Bour, O., Lavenant, N., Porel, G., Nauleau, B., Pouladi, B., et al. (2021). Numerical and experimental validation of the applicability of active-DTS experiments to estimate thermal conductivity and groundwater flux in porous media. *Water Resources Research*, *57*(1), e2020WR028078. https://doi.org/10.1029/2020WR028078

Singh, T., Gomez-Velez, J. D., Wu, L., Wörman, A., Hannah, D. M., & Krause, S. (2020). Effects of Successive peak flow events on hyporheic exchange and residence times. *Water Resources Research*, *56*(8), e2020WR027113. https://doi.org/10.1029/2020WR027113

Singh, T., Wu, L., Gomez-Velez, J. D., Lewandowski, J., Hannah, D. M., & Krause, S. (2019). Dynamic hyporheic zones: Exploring the role of peak flow events on bedform-induced hyporheic exchange. *Water Resources Research*, *55*(1), 218–235. https://doi.org/10.1029/2018WR022993

Sophocleous, M. (2002). Interactions between groundwater and surface water: The state of the science. *Hydrogeology Journal*, *10*(1), 52–67. https://doi.org/10.1007/s10040-001-0170-8

Stallman, W. (1965). Steady one-dimensional fluid flow in a semi-infinite porous medium with sinusoidal surface temperature (Vol. *70*). https://doi.org/10.1029/JZ070i012p02821

Stauffer, F., Bayer, P., Blum, P., Molina Giraldo, N., & Kinzelbach, W. (2013). Thermal use of shallow groundwater. https://doi.org/10.1201/b16239

Stonedahl, S. H., Harvey, J. W., Wörman, A., Salehin, M., & Packman, A. I. (2010). A multiscale model for integrating hyporheic exchange from ripples to meanders. *Water Resources Research*, *46*(12), W12539. https://doi.org/10.1029/2009WR008865

Storey, R. G., Howard, K. W. F., & Williams, D. D. (2003). Factors controlling riffle-scale hyporheic exchange flows and their seasonal changes in a gaining stream: A three-dimensional groundwater flow model. *Water Resources Research*, *39*(2), 1034. https://doi.org/10.1029/2002WR001367

Tonina, D., & Buffington, J. M. (2011). Effects of stream discharge, alluvial depth and bar amplitude on hyporheic flow in pool-riffle channels. *Water Resources Research*, *47*(8), W08508. https://doi.org/10.1029/2010WR009140

Tóth, J. (1963). A theoretical analysis of groundwater flow in small drainage basins. *Journal of Geophysical Research*, *68*(16), 4795–4812. https://doi.org/10.1029/JZ068i016p04795

Trauth, N., & Fleckenstein, J. H. (2017). Single discharge events increase reactive efficiency of the hyporheic zone. *Water Resources Research*, *53*(1), 779–798. https://doi.org/10.1002/2016WR019488

van de Giesen, N., Steele-Dunne, S. C., Jansen, J., Hoes, O., Hausner, M. B., Tyler, S., & Selker, J. (2012). Double-ended calibration of fiber-optic Raman spectra distributed temperature sensing data. *Sensors*, *12*(5), 5471–5485. https://doi.org/10.3390/s120505471

Woessner, W. W. (2000). Stream and fluvial plain ground water interactions: Rescaling hydrogeologic thought. *Ground Water*, *38*(3), 423–429. https://doi.org/10.1111/j.1745-6584.2000.tb00228.x

Wondzell, S. M., Herzog, S. P., Gooseff, M. N., Ward, A. S., & Schmadel, N. M. (2019). Geomorphic controls on hyporheic exchange across scales—Watersheds to particles. In *Reference module in earth systems and environmental sciences*. Elsevier. https://doi.org/10.1016/B978-0-12-409548-9.12135-9

Wörman, A., Packman, A. I., Johansson, H., & Jonsson, K. (2002). Effect of flow-induced exchange in hyporheic zones on longitudinal transport of solutes in streams and rivers. *Water Resources Research*, *38*(1), 2-1–2-15. https://doi.org/10.1029/2001WR000769

Wörman, A., Packman, A. I., Marklund, L., Harvey, J. W., & Stone, S. H. (2007). Fractal topography and subsurface water flows from fluvial bedforms to the continental shield. *Geophysical Research Letters*, *34*(7), L07402. https://doi.org/10.1029/2007GL029426

Wu, L., Singh, T., Gomez-Velez, J., Nützmann, G., Wörman, A., Krause, S., & Lewandowski, J. (2018). Impact of dynamically changing discharge on hyporheic exchange processes under gaining and losing groundwater conditions. *Water Resources Research*, *54*(12), 10076–-10093. https://doi.org/10.1029/2018WR023185

Zhang, B., Gu, K., Bayer, P., Qi, H., Shi, B., Wang, B., et al. (2023). Estimation of groundwater flow rate by an actively heated fiber optics based thermal response test in a grouted borehole. *Water Resources Research*, *59*(1), e2022WR032672. https://doi.org/10.1029/2022WR032672

Zlotnik, V., & Tartakovsky, D. M. (2018). Interpretation of heat-pulse tracer tests for characterization of three-dimensional velocity fields in hyporheic zone. *Water Resources Research*, *54*(6), 4028–4039. https://doi.org/10.1029/2017WR022476